Research Square

Preprints are preliminary reports that have not undergone peer review.
They should not be considered conclusive, used to inform clinical practice,
or referenced by the media as validated information.

Organocatalyzed Bottom-up Formation of Protocells

Oliver Trapp

oliver.trapp@cup.uni-muenchen.de

Ludwig Maximilian University of Munich https://orcid.org/0000-0002-3594-5181

Marian Ebeling

Ludwig Maximilian University of Munich https://orcid.org/0009-0009-8232-9558

Otto Berninghausen

University of Munich https://orcid.org/0000-0002-9255-0522

Khang Nguyen

University of Munich https://orcid.org/0009-0007-4492-5020

Roland Beckmann

Gene Center, LMU Munich https://orcid.org/0000-0003-4291-3898

Physical Sciences - Article

Keywords:

Posted Date: May 28th, 2025

DOI: https://doi.org/10.21203/rs.3.rs-6345142/v1

License: This work is licensed under a Creative Commons Attribution 4.0 International License.
Read Full License

Additional Declarations: There is **NO** Competing Interest.

Version of Record: A version of this preprint was published at Nature Communications on February 23rd, 2026. See the published version at https://doi.org/10.1038/s41467-026-69597-5.

Abstract

The organisation of living biological systems into cellular structures is a characteristic that enables differentiation from the environment.[1] It is assumed that a pivotal step in the development of life is compartmentalization, achieved through the formation of vesicle-like structures. Fatty acids[2-3][i]4 - or phospholipids[5] - have been used to simulate prebiotic vesicle and protocell formation. However, the mechanism by which amphiphilic molecules are formed from small prebiotically plausible molecules, which spontaneously self-assemble to protocells, remains to be elucidated.[6,7] Furthermore, a process for the selective formation of membrane molecules of defined length, such as those found in most cellular structures, remains elusive. Here we demonstrate that a reaction cascade starting from prebiotically accessible acetaldehyde under organocatalysis with prebiotic imidazolidine-4-thione rapidly yields lipid molecules that form protocells by a spontaneous self-assembly. In this process, lipids with up to C20 in length develop a membrane, which additionally incorporates the organocatalyst at the liquid-lipid interface in a self-evolutionary modification. The chemical formation and assembly were monitored by dynamic light scattering, fluorescence microscopy, (cryo)-TEM and in-situ high-resolution mass spectrometry. The size of these catalytically active vesicles and protocells ranges from ~11 nm up to 7 µm. These results demonstrate that an organocatalyst formed from prebiotic molecules such as H_2S, NH_3, H_2O, HCN and aldehydes catalyses the selective formation of lipids, facilitating spontaneous compartmentalisation. This finding unveils a novel pathway that enables protocell formation without the necessity of amphiphilic compounds being present from the start. Furthermore, we found that these protocells concentrate organic molecules and create a water-poor, lipophilic reaction environment that facilitates transformations that are difficult to achieve in water.

Introduction

Reconstructing the emergence of the first self-sustaining and self-reproducing unicellular organism is fundamental to explaining the origin of life under abiotic conditions.[8] Abiogenesis is thought to have begun with a separation from the environment by vesicles because of the advantages of compartmentalisation. Organic molecules can be concentrated in vesicles, leading to a kinetic acceleration of reactions and thus suppressing competing decomposition reactions. Although water is essential as a reaction medium for many processes, water-eliminating reactions require a reaction environment that reduces solvation by confinement in vesicles. This can favour oligomerisation reactions that take place under water elimination, such as the formation of peptides, polysaccharides or information carrying molecules such as DNA and RNA.[9,10]

In organisms, fatty acids are synthesised by the fatty acid synthase (FAS),[11] which utilizes a series of decarboxylative Claisen condensations from acetyl-CoA and malonyl-CoA (**Fig. 1a**). To simulate the formation of the first protocells (**Fig. 1b**), model vesicle systems with membranes made of monocarboxylic acids,[12,13] or phospholipids[5,14] are investigated for their properties to external stimuli such as salts, amino acids, sugars[15] or the inclusion/replication of RNA/DNA. 5[-6-78,16] Coacervates[a],[17]

are also considered to be independently plausible compartments on early Earth, as aggregation of RNA, DNA or peptides can lead to a membrane-free phase separation.[18-

Amphiphiles consisting mainly of saturated alkyl chains were proposed to originate from Fischer-Tropsch-type (FTT) reactions[23] at high temperature and pressure in geothermal vents[24] or to be of extra-terrestrial origin,[25] since alkyl carboxylic acids were found in extracts of the Murchinson meteorite.[12] Recently, the highly efficient and robust conversion of CO_2 into oxygenated organic compounds (mainly formaldehyde and acetaldehyde) by meteorite and volcanic particles has been identified over a wide range of reaction conditions.[26] Unlike the FTT reaction, no long alkanes, which are difficult to activate and convert into long-chain carboxylic acids or alcohols, were found. However, in its earliest stages, life may have developed other ways of making membranes that have been adapted to the environment over time.[27] One indicator for this hypothesis are partially unsaturated phospholipids based on geranylgeraniol, which were found in archaea.[28] Most archaean phospholipids consist of partially or fully unsaturated polyprenyl- or terpenoid-type phosphates, which can be considered as remnants of primordial vesicles.[29]

In addition to a confined reaction space, catalysis is a key element in the emergence of the first life. Without enzymes, only catalytically active minerals and metals, e.g. montmorillonite[30], magnetite[31] or reduced iron particles[26,32] were initially available on the early Earth. However, due to their insolubility, reactive heterogeneous surfaces are a poor match for separated reaction spaces. Prebiotic organocatalysts open up a wide range of reactions and can be regarded as precursors of enzymes. They not only allow selective reactions but can also be integrated into vesicles and protocells.

Recently, we found that imidazolidine-4-thiones are selectively formed from H_2S, NH_3, HCN and carbonyl compounds under mildly basic aqueous and prebiotically plausible conditions.[33] This class of compounds can be considered as thio-MacMillan type organocatalysts[34,35] capable of iminium ion or enamine catalysis. These organocatalysts are able to modify their own building blocks by a-alkylation of aldehydes under prebiotic conditions. They also dynamically exchange its substituent at C-2 with available carbonyl compounds. This self-modification can lead to new catalysts with superior properties that can outperform others. Thus, kinetic selection and evolution can occur on the molecular level.[36]

[a] ***Coacervates*** are dispersed droplets of the (short-chain) lipids that form as a result of liquid-liquid phase separation. A ***vesicle*** forms a cell-like membrane by supramolecular arrangement of lipid molecules. A ***protocell*** is a larger, spherical, self-organized, cell-like structure with a lipid membrane, which can be considered as a precursor of cells in the emergence of cellular life.

Results and Discussion

While studying prebiotic imidazolidine-4-thione organocatalysts in aldol reactions, we found that, in addition to the activation of carbonyl compounds leading to the expected aldol product, aldol-like

oligomerisation also occurs. In addition, we observed incorporation of the reaction product into the imidazolidine-4-thione, leading to a modification of the organocatalysts (**Fig. 1c**).

In particular, acetaldehyde, which is formed under prebiotic conditions from CO_2 and in-situ generated hydrogen by catalysis with meteoritic and volcanic particles, showed this organocatalyzed oligomerization.[32] For a comprehensive investigation of this process, we selected 2,5-dimethylimidazolidine-4-thione **1** (**Fig. 1c**) as prebiotic organocatalyst as it is formed in situ in the same mixture from acetaldehyde, NH_3, H_2S and KCN in water[33] (**Fig. 1d**). As these substituted imidazolidine-4-thione organocatalysts are chiral and crystallise in enantiopure crystals (conglomerate), we chose (2*RS*,5*S*)-2,5-dimethylimidazolidine-4-thione as a prebiotically formed catalyst, which can be derived from l-alanine. In initial screening experiments with varying acetaldehyde and catalyst concentrations, at a slightly acidic pH of 4, we observed that some samples became cloudy over time.

Light scattering (Supplementary Fig. S2) indicated the formation of larger assemblies. Microscopic images revealed the formation of spherical structures, and indicated a correlation between the density of these assemblies and the concentrations of the aldehyde as well as the amounts of catalyst employed. (**Fig 2a**, Supplementary Video 1).

High-resolution Orbitrap mass spectrometry (HRMS) of the suspension revealed the formation of a self-evolving organocatalytic species with extended side chains at the C-2 position or bound as iminium ion/enamine to the secondary amine as the main products, which is an intermediate of the organocatalyzed aldol oligomerization (**Fig. 1e**, Supplementary Figs. S3–4). In addition to chain elongation, unsaturated oligomers were identified. These are formed by continuous dehydration of the oligomeric polyols (Supplementary Tables S3–6). As the catalysts can be reversibly hydrolysed by ring-opening, newly formed aldehydes are incorporated by ring closing, resulting in modified organocatalysts with altered physical, chemical and catalytic properties. The product distribution of the oligomers as a function of acetaldehyde and catalyst concentration, identified by HRMS, was systematically mapped by chain length at C-2 against the dehydration steps (**Fig. 2b**). The initially added organocatalyst **1** with acetaldehyde at C-2 is located on the first data point (chain length: 2, dehydration steps: 1, Supplementary Fig. S3). This plot gives an overview of product distribution after 1 d. We observed that with increasing chain length the intensities (amount of product) initially decrease, and the degree of water elimination also increases. An increase in the aldehyde concentration resulted in a shift towards longer chains; compared to an increased catalyst loading, this trend reversed at higher catalyst loading.

The dynamic process of the oligomerising aldol addition and elimination reaction as well as the exchange reactions with the original organocatalyst **1** can be explained by the detectable intermediates on the basis of the reaction data. The interlocking catalytic cycles are summarised in **Figure 2c**. Acetaldehyde condensates on the secondary amine of the catalyst **1** to form the activated vinyl species **2**. Reaction with a second equivalent of acetaldehyde gives the first aldol addition product **3**. After hydrolysis from the catalyst, the released aldehyde **4** is now part of the aldehyde pool. It can react in the same way with another vinyl species **2** to elongate the oligomeric chain **5** and be released as aldehyde **6**.

Interestingly, the mechanism we propose is similar to the well-known mitochondrial fatty acid synthesis, in that new C_2-units are not inserted at the end of the chain, but at the beginning.[37] Favoured by the lowered pH, an elimination of water to form an unsaturated lipid chain **7** can occur after every aldol addition. As the catalyst is in small equilibrium with the hydrolysed open ring form **8**, free aldehydes can be incorporated. This may result in the natural selection of certain products due to their enhanced stability towards hydrolysis. The newly formed organocatalysts are catalytically active, exhibiting modified selectivity towards the substrate due to modified sidechains, thereby instigating an evolutionary process within the system.

A systematic investigation into external factors, pH dependency and salt concentrations were undertaken to gain further mechanistic insight. The titration curve of the catalyst showed amphoteric characteristics (Supplementary Fig. S1). The determined pK_a values of the thiolactam (pK_{a1} = 3.8) and secondary amine (pK_{a2} ~11) in aqueous solution showed that the catalyst can buffer the solution at pH 4 which is the optimal reaction condition for the enamine formation. This finding serves to demonstrate the necessity of the thiolactam and underscores its pivotal role in ensuring the maintenance of the optimal pH range. In comparison, lactams are considerably less acidic (ΔpK_a = +6) and therefore cannot buffer the reaction at pH 4.[38,39]

When the pH of the reaction was reduced to 2.5, no change in HRMS data was observed, whereas the assembly formation decreased in microscope micrographs. Conversely, an increase to pH 7, resulted in the detection of shorter oligomers by HRMS, accompanied by a reduction in water elimination (Supplementary Table S21). This outcome is consistent with the notion that enamine formation and water elimination are favoured under acidic conditions.

When adding the salts NaCl (0.4 m) or $MgCl_2$ (0.01 m) to simulate an early ocean environment resulted in an increased reaction rate, enhanced water elimination, and the formation of longer oligomers (Supplementary Table S15). However, the presence of high concentrations of NaCl led to a significant inhibition of the self-assembly process, as observed by light microscopy analysis. Conversely, the organocatalytic system exhibited persistent assembly after 3 days in reactions with $MgCl_2$, suggesting that it functions optimally at lower salt concentrations. It is also noteworthy that the assemblies demonstrated tolerance to $MgCl_2$. In comparison, fatty acids or phosphates are more susceptible to M^{2+} metal ions as membrane formation is generally disrupted by them. [8,40,41]

In order to ascertain the robustness of our reaction system over time, a wide range of conditions were monitored by time resolved HRMS (Supplementary Table S3-6) and microscopy (Supplementary Table S10-13). To achieve higher reaction rates over the observed time span, higher concentrations, i.e. 1 m acetaldehyde and 10 mol% catalyst, were selected as a suitable model system. This facilitated the observation of the reaction progressing from a state of low particle count to an exponential increase over the course of 1 d (**Fig. 3a**, see also Supplementary Video 2). During this process, an increase in the maximum chain length from 14 to 20, as well as a general increase in abundance of shorter chain

lengths, was observed, showing the dynamic growth of the oligomers over time (**Fig. 3b**). It is a well-established principle that, in general, the abundance of a given substance decreases with increasing chain length. This phenomenon can be attributed to the dynamic change of selectivity by decreasing solubility and phase transition from dissolved liquids to lipids with increasing oligomeric chain length.[42] Furthermore, an increase in oligomeric chain length over C20 was not observed in timeframes of up to 7 d, which is a remarkable result as it indicates that the selectivity of the chain length of the lipid chains observed in living biological systems between C16 and C20 may have its origin in the physical properties, namely the solubility in the water phase and the ability to form stable membranes by van-der-Waals interactions of the organic chain and self-assembly. Interestingly, a heterogeneous distribution of chain lengths can facilitate the self-assembly of vesicles.[43, 44] In comparison, the aldol oligomerization in toluene catalysed by a cation exchange resin yields significantly larger oligomers.[45] It is noteworthy that at the inception of the reaction, the presence of hydrated chains was observed. However, over time, a shift towards a greater proportion of unsaturated lipid chains becomes evident, attributable to the irreversible elimination of water during the reaction.

To illuminate growth of the assemblies over time, a dynamic light scattering (DLS) experiment was performed. For a side-by-side comparison, we used the same reaction conditions as in **Figure 3a** to determine the median hydrodynamic diameter D_h of particles in solution and track changes as the reaction advances (**Fig. 3b-e**). Initially, predominantly assemblies of approximately 100 nm in diameter were observed which underwent growth over 6 h up to a limit of »800 nm (**Fig. 3c**). This observation is consistent with the observation in **Figure 3a**, that after 1 h nearly no macromolecular structures were observed, as the formed assemblies were yet too small for microscopic observation. Concurrently, the DLS experiment detected the emergence of larger assemblies in the µm-range, whose significant increase in numbers can also be observed in the micrographs from 6 h onward (**Fig. 3d,e**).

In order to further understand the emergence and properties of the nm-scale particles, transmission electron microscopy (TEM) was used. Initially, TEM negative stains were obtained of dried samples using uranyl acetate for contrast (Supplementary Fig. S7). This analysis yielded a diverse array of spheres ranging from 60 nm up to 2.0 µm in size, depending on reaction time (**Fig. 4a)**. Negative staining gives only the outline of the assemblies and provides little information about the structure itself.

Consequently, the assembly boundaries were investigated in solution by cryo-TEM (Supplementary Fig. S8-9). The structure of the particles was visualised by vitrification of the reaction mixture (**Fig. 4b,c**). Here, we found spherical structures ranging in size from approximately 11 nm to 1.5 µm, which is consistent with the measurements of the negative stain and the DLS experiment. The structure depicted in **Fig. 4b** is characterised by a distinct boundary, though the presence of a double membrane remains undetectable. Of particular interest are the dark spheres observed within the structure, which are indicative of local water accumulation. This water accumulation is a significant indication of the formation mechanism of the protocells formed (vide infra). These results suggest the formation of coacervates in the initial phase. Furthermore, significantly smaller spheres were observed (**Fig. 4c**). Due to the small size (11–40 nm) and the resolution limit, a definitive evaluation of the boundary region

remains unfeasible. However, measurements of the boundary region resulted in a theoretical thickness of 3.1 ± 0.2 nm independent of the sphere diameter, which implicates a bilayer (Supplementary Fig. S10, Supplementary Table S23). In comparison, the bilayer formed by decanoic acid is 1.4–1.5 nm[46] and of phosphatidylcholines 1.5–3.7 nm.[47] In addition to the time-frozen cryo-TEM study, we also wanted to investigate possible dynamic processes, as permeability, accumulation and growth in the compartments are essential for the development of living cells.

Fluorescence microscopy using rhodamine B as a fluorescent probe for non-polar membranes showed that the entire sphere was uniformly illuminated (see **Fig. 4d**). As the dye was added immediately before the measurement, it can be concluded that the boundary was permeable to rhodamine B. In general, fluorescence is quenched less in more nonpolar environments, providing a contrast to the surrounding polar water.[48] This phenomenon is used, for example, to observe non-polar regions in bilayers or coacervates.[49] As the inside of the spheres is significantly brighter, the spheres are composed of an internally uniform non-polar medium, unlike normal vesicles, which contain water. We therefore conclude that a coacervate-like structure is the best approximation for the found results, as deduced from the previous experiments. We propose that an interface to the surrounding water is formed by the amine of the five-membered ring of the evolved catalyst which is protonated at the lowered pH. This head group can interact with the surrounding water, while the side chains point into the non-polar interior (**Fig. 4g**).

Subsequent observation of the fluorescence of the assemblies over time reveals the emergence of small dark spherical areas, which grow and merge within the interior (Supplementary Video 3, **Fig. 4e**). The higher fluorescence quenching suggests a more polar medium compared to pure water. This observation is plausible since during the catalytic cycle dehydration in the aldehyde/catalyst pool continuously produces water (**Fig. 2c**). These dark spheres were also observed in the cryo-TEM **Fig. 4b** (Supplementary Fig. S8-9).

The observed increase in fluorescence intensity in the non-polar phase indicates that the phase even becomes increasingly non-polar as the elimination of water and the conversion of the polyols to polyenes proceed. The formed water is immiscible with the non-polar medium and concentrates on the inside, thermodynamically driven, in a second phase as small droplets, which combine over time and are even emptied to the outside of the sphere in some cases (Supplementary Video 4-5). To assess the impact of local warming of the sample during fluorescence microscopy, a reaction was conducted at 40 °C (Supplementary Table S16-17). Fluorescence microscopy revealed an increase in the overall particle size (up to 7 µm) and an accumulation of water within the sphere. Previously this phenomenon was predominantly observed during extended periods of fluorescence microscopy observations. Consequently, it can be concluded, that elevated temperatures, or local irradiation result in enhanced conversion, thereby facilitating water elimination. In comparison, a test reaction conducted at 0 °C did not exhibit these characteristics and light micrographs as well as HRMS measurements indicated a decelerated reaction (Supplementary Table S19-20).

Phase separation and excretion of water plays a pivotal role in the progress of a first chemical metabolism, as water is constantly removed from equilibrium. This process further facilitates the elimination of alcohols in the sidechain, leading to the formation of more nonpolar chains, and supports the exchange reaction of the aldehydes with the catalyst. This behaviour may have facilitated the concentration of nonpolar molecules and driven forward condensation reactions with other compounds, which are difficult in a purely aqueous system.

However, should the formed water not be shuttled outside, then all water droplets will combine over time. The resultant protocell structure exhibited encapsulation of water by a thin layer of non-polar medium (**Fig. 4f**). The hypothesis is thus put forward that the evolved amphiphilic catalysts adapt to form a double layer due to internal water accumulation. This finding is extraordinary, as the formed protocell generated its membrane and water content from within itself, which is a so far unknown and unique process to a self-assembled protocell formation. This observation may provide an explanation for the transition from coacervates via vesicle-like structures to protocells that occurred on Earth in the early stages of its evolution. This principle can be theoretically transferred to similar reaction systems. The formation of protocells marks a significant milestone in the evolution of life on Earth. Given the dye's ability to permeate the coacervates, it can be deduced that other organic compounds must also be capable of doing so, leading to their accumulation within the vesicle.

Conclusion

In summary, a lipid oligomer formation reaction was identified as a key step in the process that leads to the self-assembly of molecules, the formation of coacervates, and ultimately the development of protocells. This process, which commences with small molecules such as acetaldehyde, does not necessitate the use of detergents or lipid precursors. Remarkably, the lipids produced in this organocatalyzed aldol reaction and condensation cascade have lengths of up to C20, which is similar to those found in biological systems.

The organocatalytic reaction cycle was elucidated, and a mechanism involving interlocking catalytic reaction cascades was proposed. The imidazolidine-4-thione organocatalysts are prebiotically plausible, as they are formed in high yield from small molecules (acetaldehyde, hydrogen sulphide, ammonia, and cyanides) that were abundant on early Earth. These organocatalysts exhibit a unique property: the ability to undergo molecular evolution through the catalytic modification of their own building blocks, in this case aldehyde precursors, and assimilation into their own structure.

This previously unknown process of lipid formation, self-assembly and self-modification of the initial catalyst was experimentally observed. The distinct catalytic modification of the resulting lipids leads to the catalytic activation of the entire surface of the resulting protocells. The physical properties, size, and formation of the coacervates, their transition to vesicles and protocell structures were characterised by fluorescence microscopy, DLS experiments, and cryo-TEM. The smallest structures found were about 11 nm, and the largest reached up to 7 µm. Time-resolved fluorescence experiments showed the

incorporation of the dye rhodamine B and internal water production by condensation reactions, leading to the transformation of coacervates into protocells.

This process is stable and reproducible over a wide range of reaction conditions, including varying concentrations, pH, temperature, and salts. An interesting feature of the initially formed coacervates and final protocells is the accumulation of organic compounds through the lipid membrane. As a result, the concentration ratios change rapidly, as the organic molecules in these self-assemblies can be concentrated to a higher level. Once started, this feature would also allow for the reactions to progress in prebiotic environments with low concentrations of potential organic substrates. Combined with the catalytically active surface, this leads to an exponential formation of protocells, as observed in the in-situ microscopic tracking of the protocell formation. These conditions may also favour condensation reactions in general, such as the oligomerisation of RNA.

Our results show that it is possible to form the first macromolecular structures from simple molecules under abiotic reaction conditions, without the need for a harsh environment or extraterrestrial supply of materials. These protocells are an excellent starting point for further research into the emergence of life, as they form under the simplest reaction conditions and simultaneously solve many challenging problems, such as the concentration of organic compounds, while providing a protected reaction space for the formation of life-relevant molecules.

Declarations

Data availability

All data generated or analysed during this study are included in this published article (and its Supplementary Information Files).

Acknowledgments We thank the Max - Planck Society (Max - Planck - Fellow Research Group ‘Origins of Life’, OT), Germany's Excellence Strategy, ORIGINS, EXC – 2094 – 390783311 (OT), DFG/German Research Foundation, Project – ID 521256690 – TRR 392, Molecular Evolution (OT), and the Volkswagen Stiftung, Initiating Molecular Life (OT) for funding.

Author contributions M.S.R.E. and O.T. conceived and designed the experiments. M.S.R.E. and K.H.N. performed the experiments. M.S.R.E. and O.B. performed microscopy and (cryo-) TEM experiments. M.S.R.E., O.B., R.B., and O.T. analysed the data. M.S.R.E., O.B., R.B., and O.T. wrote the paper. All authors discussed the results and commented on the manuscript.

Competing interests

The authors declare no competing interests.

Additional information
Supplementary information The online version contains supplementary material available at

https://doi.org/XX

References

1. Sharma, Aet alAssembly theory explains and quantifies selection and evolutionNature 622, 321-328 (2023).
2. Deamer, DWBoundary structures are formed by organic components of the Murchison carbonaceous chondriteNature 317, 792-794 (1985)https://doi.org/10.1038/317792a0
3. Kindt, JT., Szostak, JW.& Wang, ABulk self-assembly of giant, unilamellar vesiclesACS Nano 14, 14627-14634 (2020).
4. Zozulia, Oet alAcyl phosphates as chemically fueled building blocks for self-sustaining protocellsAngewChemIntEd63, e202406094 (2024).
5. Toparlak, ÖDet alCyclophospholipids Enable a Protocellular Life CycleACS Nano 17, 23772-23783 (2023)https://doi.org/10.1021/acsnano.3c07706
6. Podolsky, KA.& Devaraj, NKSynthesis of lipid membranes for artificial cellsNature RevChem5, 676-694 (2021).
7. Ivanov, Iet alBottom-up synthesis of artificial cells: recent highlights and future challengesBioorgMedChemLett12, 287-308 (2021).
8. Szostak, JW., Bartel, DP.& Luisi, PLSynthesizing lifeNature 409, 387-390 (2001).
9. Ruiz-Mirazo, K.; Briones, C.; Escosura, ADL., Prebiotic Systems Chemistry: New Perspectives for the Origins of LifeChemRev2014, 114, 285-366.
10. Nogal, N.; Sanz-Sánchez, M.; Vela-Gallego, S.; Ruiz-Mirazo, K.; Escosura, ADL., The protometabolic nature of prebiotic chemistryChemSocRev2023, 52, 7359-7388.
11. Wakil, SJ., Toops, JKS.& Joshi, VCFatty acid synthesis and its regulationAnnuRevBiochem52, 537-579 (1983).
12. Lawless, JG& Yuen, GUQuantification of monocarboxylic acids in the Murchison carbonaceous meteoriteNature 282, 396-398 (1979)https://doi.org/10.1038/282396a0
13. Walde, P., Wick, R., Fresta, M., Mangone, A.& Luisi, PLAutopoietic self-reproduction of fatty acid vesiclesJAmChemSoc116, 11649-11654 (1994).
14. Dreher, Y., Jahnke, K., Bobkova, E., Spatz, JP.& Göpfrich, KDivision and regrowth of phase-separated giant unilamellar vesiclesAngewChemIntEd60, 10661-10669 (2021)https://doi.org/10.1002/anie.202014174
15. Todd, ZR., Cohen, ZR., Catling, DC., Keller, SL& Black, RAGrowth of Prebiotically Plausible Fatty Acid Vesicles Proceeds in the Presence of Prebiotic Amino Acids, Dipeptides, Sugars, and Nucleic Acid ComponentsLangmuir 38, 15106-15112 (2022)https://doi.org/10.1021/acs.langmuir.2c02118
16. Adamala, K& Szostak, JWNonenzymatic Template-Directed RNA Synthesis Inside Model ProtocellsScience 342, 1098-1100 (2013)https://doi.org/10.1126/science.1241888

17. Oparin, AI& Gladilin, KLEvolution of self-assembly of probiontsBiosystems 12, 133-145 (1980)https://doi.org/10.1016/0303-2647(80)90011-8
18. Tang, T-Y.Det alFatty acid membrane assembly on coacervate microdroplets as a step towards a hybrid protocell modelNature Chemistry 6, 527-533 (2014)https://doi.org/10.1038/nchem.1921
19. Qiao, Y., Li, M., Booth, R& Mann, SPredatory behaviour in synthetic protocell communitiesNature Chemistry 9, 110-119 (2017)https://doi.org/10.1038/nchem.2617
20. Aumiller, WM& Keating, CDPhosphorylation-mediated RNA/peptide complex coacervation as a model for intracellular liquid organellesNature Chemistry 8, 129-137 (2016)https://doi.org/10.1038/nchem.2414
21. Aumiller, WM., Pir Cakmak, F., Davis, BW& Keating, CDRNA-Based Coacervates as a Model for Membraneless Organelles: Formation, Properties, and Interfacial Liposome AssemblyLangmuir 32, 10042-10053 (2016)https://doi.org/10.1021/acs.langmuir.6b02499
22. Chen, IA& Walde, PFrom self-assembled vesicles to protocellsCold Spring HarbPerspectBiol2, a002170 (2010).
23. Nooner, DW.& Oro, JSynthesis of fatty acids by a closed system Fischer-Tropsch process (hydrocarbon synthesis from carbon monoxide and hydrogen)Advances in Chemistry 178, 159-171 (1979).
24. Rushdi, AI.& Simoneit, BRTLipid Formation by Aqueous Fischer-Tropsch-Type Synthesis over a Temperature Range of 100 to 400 °COrigins of life and evolution of the biosphere 31, 103-118 (2001)https://doi.org/10.1023/A:1006702503954
25. Cohen, ZRet alPlausible sources of membrane-forming fatty acids on the early earth: A review of the literature and an estimation of amountsACS Earth Space Chem7, 11-27 (2023).
26. Peters, S., Semenov, DA., Hochleitner, R& Trapp, OSynthesis of prebiotic organics from CO2 by catalysis with meteoritic and volcanic particlesScientific Reports 13 (2023)https://doi.org/10.1038/s41598-023-33741-8
27. Krishnamurthy, RLife's Biological Chemistry: A Destiny or Destination Starting from Prebiotic Chemistry? Chemistry – A European Journal 24, 16708-16715 (2018)https://doi.org/10.1002/chem.201801847
28. Hafenbradl, D., Keller, M., Thiericke, R& Stetter, KOA Novel Unsaturated Archaeal Ether Core Lipid from the Hyperthermophile Methanopyrus kandleriSystematic and Applied Microbiology 16, 165-169 (1993)https://doi.org/10.1016/S0723-2020(11)80463-7
29. Ourisson, G.& Nakatani, YThe terpenoid theory of the origin of cellular life: the evolution of terpenoids to cholesterolChemistry & Biology 1, 11-23 (1994)https://doi.org/10.1016/1074-5521(94)90036-1
30. Ferris, JP& Ertem, GOligomerization of Ribonucleotides on Montmorillonite: Reaction of the 5'-Phosphorimidazolide of AdenosineScience 257, 1387-1389 (1992)https://doi.org/10.1126/science.1529338

31. Preiner, Met alA hydrogen-dependent geochemical analogue of primordial carbon and energy metabolismNature Ecology & Evolution 4, 534-542 (2020).
32. Muchowska, KB., Varma, SJ.& Moran, JSynthesis and breakdown of universal metabolic precursors promoted by ironNature 569, 104-107 (2019).
33. Closs, AC., Fuks, E., Bechtel, M& Trapp, OPrebiotically Plausible Organocatalysts Enabling a Selective Photoredox α-Alkylation of Aldehydes on the Early EarthChemistry – A European Journal 26, 10702-10706 (2020)https://doi.org/10.1002/chem.202001514
34. Ahrendt, KA., Borths, CJ.& MacMillan, DWCNew strategies for organic catalysis: the first highly enantioselective organocatalytic Diels–Alder reactionJAmChemSoc122, 4243-4244 (2000).
35. Beeson, TD., Mastracchio, A., Hong, J-B., Ashton, K.& MacMillan, DWCEnantioselective organocatalysis using SOMO activationScience 316, 582-585 (2007).
36. Closs, AC., Bechtel, M& Trapp, ODynamic Exchange of Substituents in a Prebiotic Organocatalyst: Initial Steps towards an Evolutionary SystemAngewandte Chemie International Edition (2021)https://doi.org/10.1002/anie.202112563
37. Wedan, RJ., Longenecker, JZ& Nowinski, SMMitochondrial fatty acid synthesis is an emergent central regulator of mammalian oxidative metabolismCell Metabolism 36, 36-47 (2024)https://doi.org/10.1016/j.cmet.2023.11.017
38. Bordwell, FGEquilibrium acidities in dimethyl sulfoxide solutionAccChemRes21, 456-463 (1988).
39. Mahanta, N., Szantai-Kis, DM., Petersson, EJ.& Mitchell, DABiosynthesis and chemical applications of thioamidesACS ChemBiol14, 142-163 (2019).
40. Monnard, PA& Deamer, DWMembrane self-assembly processes: Steps toward the first cellular lifeThe Anatomical Record 268, 196-207 (2002)https://doi.org:10.1002/ar.10154
41. Monnard, P-A., Apel, CL., Kanavarioti, A.& Deamer, DWInfluence of ionic inorganic solutes on self-assembly and polymerization processes related to early forms of life: implications for a prebiotic aqueous mediumAstrobiology 2, 139-152 (2002).
42. Ralston, AW.& Hoerr, CWThe solubilities of the normal saturated fatty acidsJOrgChem07, 546-555 (1942).
43. Cape, JL., Monnard, P.-A& Boncella, JMPrebiotically relevant mixed fatty acid vesicles support anionic solute encapsulation and photochemically catalyzed trans-membrane charge transportChemical Science 2, 661 (2011)https://doi.org/10.1039/c0sc00575d
44. Budin, I., Prywes, N., Zhang, N& Szostak, W., JackChain-Length Heterogeneity Allows for the Assembly of Fatty Acid Vesicles in Dilute SolutionsBiophysJ107, 1582-1590 (2014)https://doi.org/10.1016/j.bpj.2014.07.067
45. Kamal, S.& Mahajani, SKinetic study for oligomerization of acetaldehyde over cation exchange resinApplMicrobiolBiotechnol608, 117841 (2020).
46. Sepulveda, RVet alInsights into early steps of decanoic acid self-assemblies under prebiotic temperatures using molecular dynamics simulationsMembranes 13, 469 (2023).

47. Lewis, BA.& Engelman, DMLipid bilayer thickness varies linearly with acyl chain length in fluid phosphatidylcholine vesiclesJMolBiol166, 211-217 (1983).
48. Ma, YFluorescence Characteristics Analysis of Rodamine BJournal of Physics: Conference Series 2468, 012022 (2023)https://doi.org/10.1088/1742-6596/2468/1/012022 ; Maillard, Jet alUniversal quenching of common fluorescent probes by water and alcoholsChemical Science 12, 1352-1362 (2021)https://doi.org/10.1039/d0sc05431c ; Dobretsov, GE., Syrejschikova, TI& Smolina, NVOn mechanisms of fluorescence quenching by waterBiophysics 59, 183-188 (2014)https://doi.org/10.1134/s0006350914020079
49. Ji, Y.& Qiao, YTuning interfacial fluidity and colloidal stability of membranized coacervate protocellsCommunications Chemistry 7, 122 (2024).

Figures

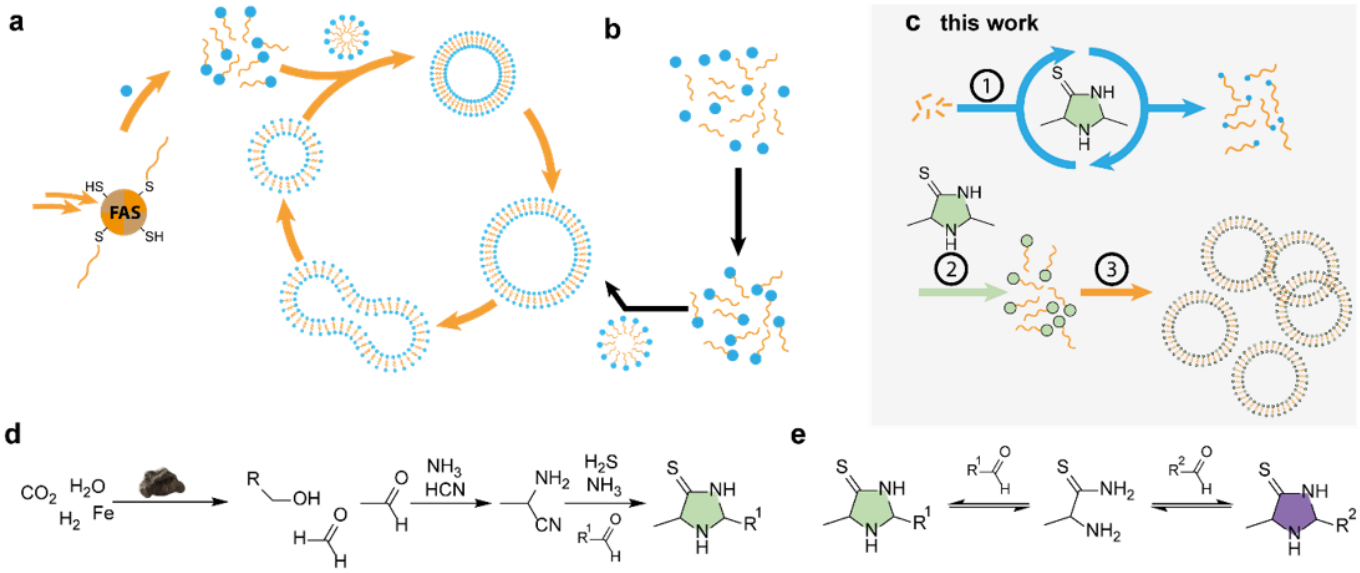


Figure 1

Lipid forming reactions and self-assembly of lipid molecules to vesicles and protocells. a, Biological synthesis of fatty acids by fatty acid synthase (FAS). b, In-situ generation of artificial protocells using amphiphilic lipids and precursor molecules to release the lipids by reaction. c, Organocatalytic oligomerization starting from small molecules (step 1), i.e. acetaldehyde, self-modification of the organocatalyst with the in-situ formed amphiphilic molecules (step 2), and self-assembly to protocells (step 3). d, prebiotic synthesis of imidazolidine-4-thione organocatalysts. e, dynamic exchange of C-2 aldehyde substituent leading to modified organocatalysts.

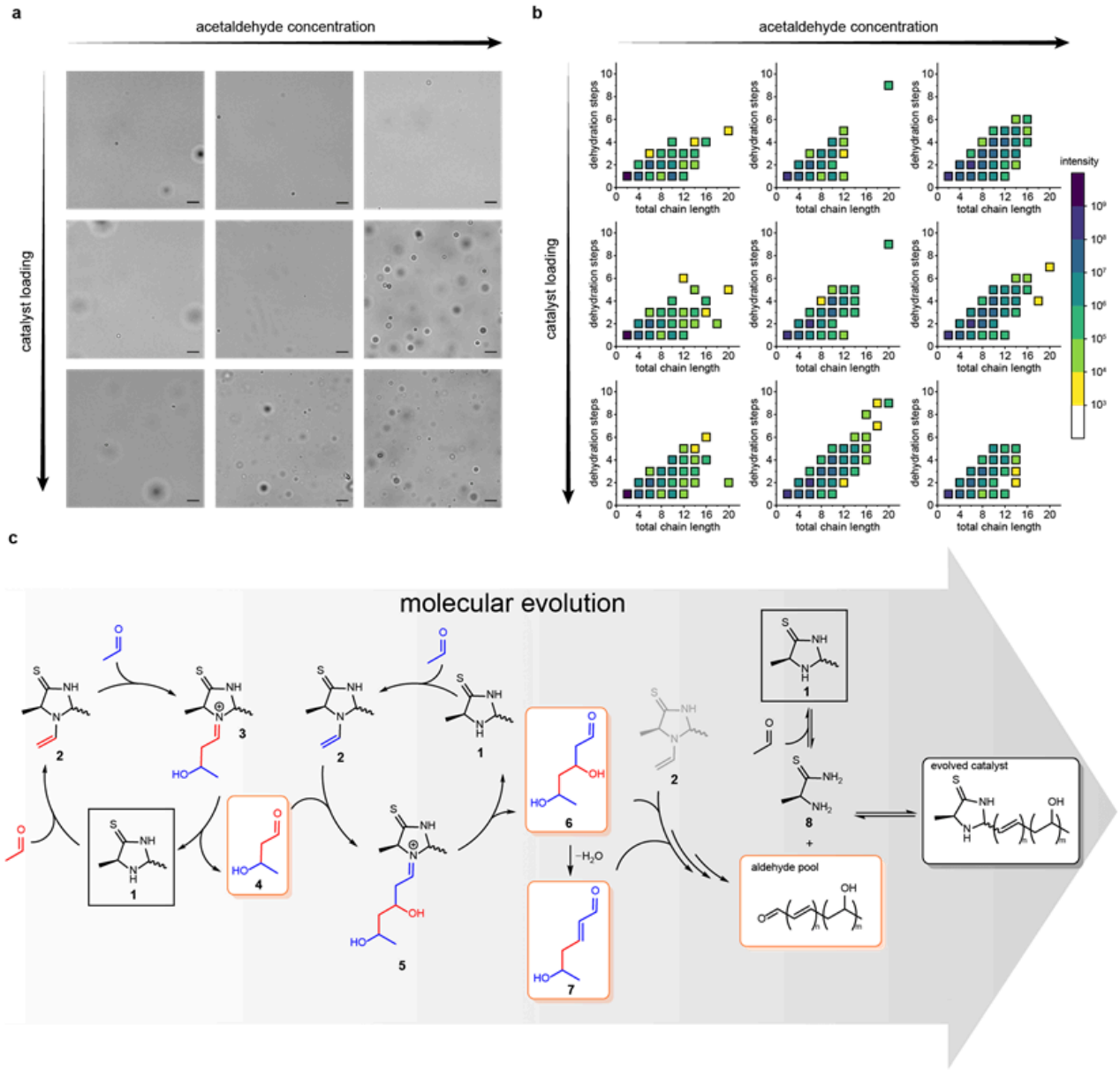


Figure 2

Concentration screening and proposed reaction mechanism. a, Micrographs of an aqueous solution. Scale bar: 10 μm. b, Extracted HRMS data of catalyst-masses with chain lengths of 2–20 plotted against dehydration grade extracted for $[M+H]^+$. Reaction conditions for a and b: 0.2, 0.5 or 2.0 m acetaldehyde from left to right, with 1, 10 or 20 mol% catalyst loading from top to bottom after 1 d. Sample dilution was referenced to catalyst concentration for every acetaldehyde concentration. c, Proposed interlocking catalytic cascade of organocatalysed aldol oligomerization reaction and molecular evolution of the catalyst.

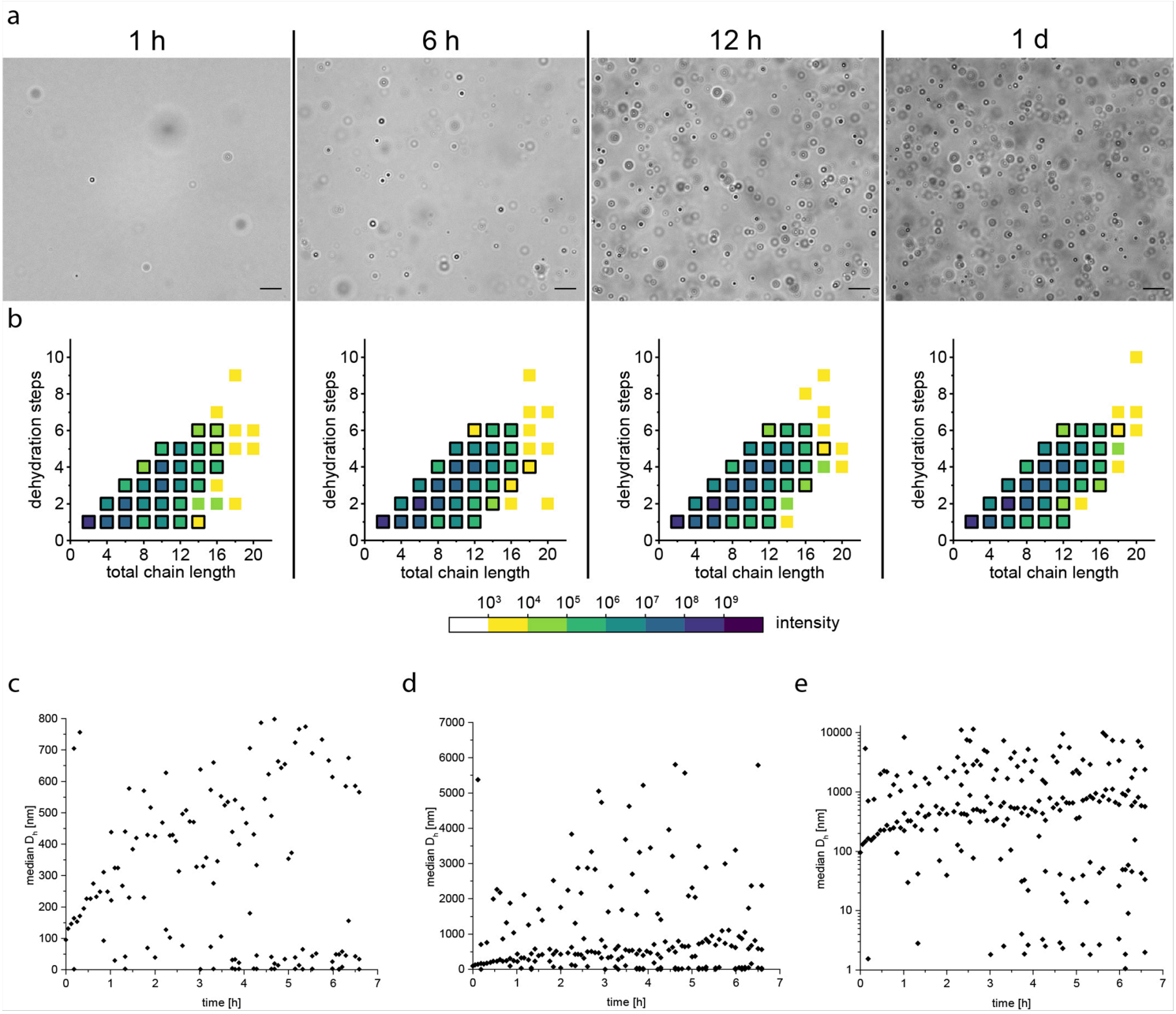


Figure 3

Dynamic processes during the reaction at 1.0 m acetaldehyde with 10 mol% catalyst loading over time. a, Micrographs taken after 1 h, 6 h, 12 h and 1 d. Scale bar: 10 µm. HRMS-data of catalyst chain length composition extracted for $[M+H]^+$ after 1 h, 6 h, 12 h and 1 d. The reaction was repeated three times and the intensities averaged for every data point. For data points with a black border, the calculated mass was found in every measurement. The micrographs did not vary between samples. For a detailed figure including the variation coefficient see Supplementary Table S7-9. c, d, and e, Dynamic light scattering (DLS) plots of the median hydrodynamic radius D_h of particles found up to 800 nm (c), 7 µm (d) and log-scale up to 10 µm (e), respectively, against the time at 1.0 m acetaldehyde with 10 mol% catalyst loading. Data points smaller than 1 nm were omitted due to solvent effects.

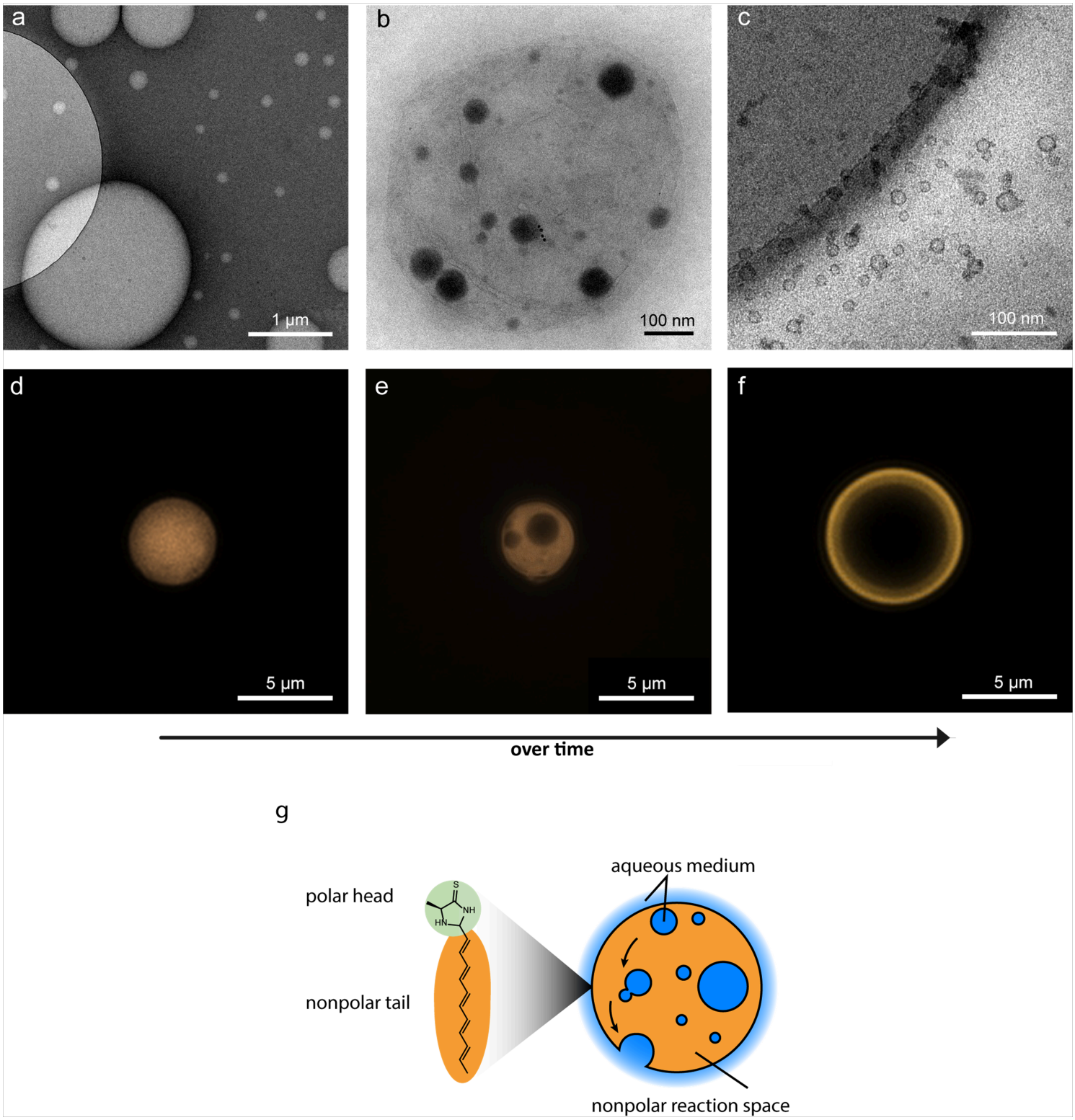


Figure 4

(cryo)-TEM micrographs and fluorescence microscopy. a, Negative stain using uranyl acetate of a reaction starting with 0.2 m acetaldehyde and 5 mol% catalyst loading after 6 h. Scale bar: 1 µm. The uniform partial circle is a hole in the holey carbon-supported grid. b,c, Cryo-TEM image of a reaction using 0.5 m acetaldehyde with 5 mol% catalyst loading after 1 h. Scale bar: 100 nm. A water enriched coacervate (b) and significantly smaller structures (c) are visible. d, e, and f, Fluorescence microscopy of

a reaction using 0.5 m acetaldehyde with 5 mol% catalyst loading developing over time. Orange: nonpolar probe rhodamine B. Scale bar: 5 μm. d, Initial coacervate formation. e, Coacervate with water accumulation. f, Protocell structure. g, Proposed model for protocell formation.

Supplementary Files

This is a list of supplementary files associated with this preprint. Click to download.

- Video1.gif
- Video2.mov
- SIGuideV2.docx
- Video3.mov
- Video4.mov
- Video5.mov
- SIV19.pdf